Russian Journal of Earth Sciences

Internal Tides North of the Critical Latitude in the Fram Strait

E. G. Morozov* **and D. I. Frey**

Shirshov Institute of Oceanology RAS, Moscow, Russia
* **Correspondence to:** Eugene Morozov, egmorozov@mail.ru

Abstract: We analyze measurements of temperature on moorings in the Fram Strait. Locations of moorings differ by the slope of the bottom topography and efficient vorticity induced by mean currents in the strait. Forcing by tidal currents also differs in different regions of the strait. High negative (anticyclonic) vorticity occasionally allows existence of internal tides of the M_2 frequency north of the critical latitude (74°30' N) for these waves.

Keywords: moorings, Fram Strait, internal tides, critical latitudes, vorticity.

Citation: Morozov E. G., Frey D. I. (2025), Internal Tides North of the Critical Latitude in the Fram Strait, *Russian Journal of Earth Sciences*, 25, ES5005, EDN: ILUMXN, https://doi.org/10.2205/2025es001050

Introduction

Internal tides are generated when currents of the tide overflow irregularities of the bottom topography. A vertical component of tidal currents appears over bottom slopes. This component periodically displaces isopycnals; thus, internal tides are generated [*Baines*, 1982; *Garrett and Kunze*, 2007; *Morozov*, 1995; *Prinsenberg et al.*, 1974]. Usually, the most energetic currents of the barotropic tide are associated with the frequency corresponding to the barotropic tide M_2 with a period of 12.4 h. This process is common at low and mid-latitudes, but at high latitudes generation of the M_2 internal tide is different. The influence of Earth's rotation plays a critical role at Arctic latitudes. Let us show this on the example of a differential equation of the second order for vertical velocities w caused by internal waves [*Krauß*, 1966; *LeBlond and Mysak*, 1978; *Tareev*, 1966]:

$$\frac{d^2w}{dz^2} + \frac{N^2(z)}{g}\frac{dw}{dz} + \frac{N^2(z) - \omega^2}{\omega^2 - f^2}k^2 w = 0. \tag{1}$$

Here, k is the wavenumber, ω is the frequency of the M_2 tide. We assume that the boundary conditions for the vertical velocity are zero at the surface and bottom. This equation is valid if the bottom is flat. If we study internal waves at high-latitudes, the denominator in the third term of this equation becomes extremely important. The difference between the M_2 tidal frequency and the Coriolis parameter decreases with increasing latitude. Approximately at latitude 74°30', this difference becomes equal to zero; hence oscillatory solutions of Equation 1 such as

$$w(z) = A(z)\sin(k_z z + \varphi)$$

in the linear formulation do not exist.

Thus, at latitudes north of 74°30' internal tides with a period of 12.4 h (M_2 frequency) cannot exist. However, the generation of internal tides at high latitudes does not differ from a similar process at low latitudes. The currents of the barotropic tide flow over underwater slopes regardless of latitude and periodically displace isopycnal surfaces up and down due to the appearance of vertical components of these currents near submarine slopes [*Baines*, 1982; *Khimchenko et al.*, 2020; *Konyaev and Sabinin*, 1992; *Morozov et al.*, 2020].

Research Article

Received: June 12, 2025
Accepted: July 30, 2025
Published: September 10, 2025

The differences between the behavior of internal tides at lower and higher latitudes appear because the wave cannot propagate from the slope in the region of super-critical latitudes and becomes a forced wave only over a submarine slope.

The difference between high and low latitudes is seen from an example of the numerical modeling of generation and propagation of the M_2 internal tide at latitudes of 78° N and 20° N [*Morozov and Pisarev*, 2002, 2023]. At high latitude, only forced wave exists over the slope and decays when propagating over flat bottom. At low latitude, the wave generated over the slope propagates from the slope. All parameters were the same in the numerical simulation except for latitudes.

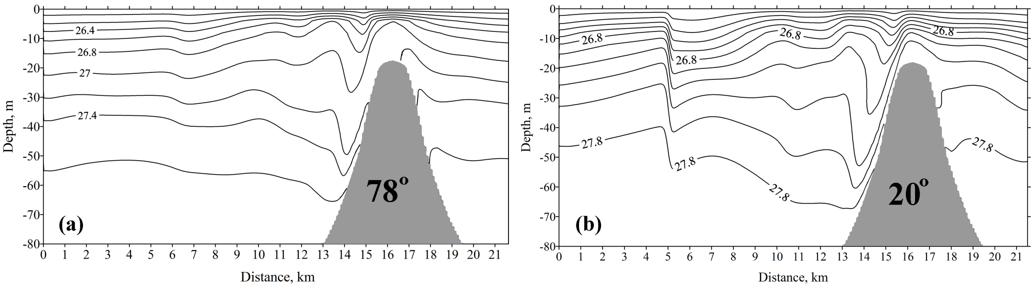

Figure 1. Model calculation of isotherms fluctuating with a frequency of the M_2 tide at latitudes 78° N (a) and 20° N (b).

Krauß [1966] was probably the first who reported in a well-known monograph about one of the first observations of internal tides at high latitudes. He described the observations during several days from an anchored ship at a station in the Barents Sea. An example of the existence of internal tide north of 75° N was described, although in the same book Krauss presents a theoretical result that free internal waves with the M_2 tidal period cannot exist north of the critical latitude. Later, other observations of the existence of such waves at high latitudes were reported in [*Konyaev et al.*, 2000; *Levine et al.*, 1985; *Marchenko and Morozov*, 2016; *Morozov and Frey*, 2023; *Parsons et al.*, 1996; *Plueddemannn et al.*, 1998].

Several explanations exist about the causes of the existence of internal tides north of the critical latitude. One of them is a decrease in the efficient Coriolis frequency. This decrease can be caused by background negative (anticyclonic) vorticity. The efficient inertial frequency is determined by the combination of the planetary vorticity and vorticity of the field of currents, which strongly depends on the eddies existing in the region.

The efficient Coriolis frequency is presented as

$$f_{\text{eff}} = f_{\text{local}} + \text{vorticity} = f_{\text{local}} + \left(\frac{dv}{dx} - \frac{du}{dy}\right).$$

Here, $f_{\text{local}} = 2\Omega \sin\varphi$ at latitude φ; Ω is the angular velocity of the Earth's rotation. If vorticity is negative (anticyclonic) the efficient Coriolis frequency becomes smaller; hence, the difference $(\omega - f)$ is positive.

It was shown by *Kozubskaya et al.* [1999] that negative vorticity up to $5.5 \times 10^{-6}\ \text{s}^{-1}$ observed in the ocean can displace the efficient critical latitude up to the latitudes of Spitsbergen (78° N). The authors described the Barents Sea Polar Front experiment in August 1992, which included a CTD-survey of 72 stations over a square limited by 77.0°–74.8° N, 21.0–24.0° E. The study site was located exactly at the critical latitude for the M_2 internal tide. Three moorings were deployed in the region. One of the goals of research was to analyze internal waves in the region.

Another possible cause of the existence of internal tides at high latitudes is sloping bottom. Semidiurnal internal tides of the M_2 frequency are frequently observed over underwater slopes. This phenomenon was shown by *Pisarev* [1988, 1991, 1992]. *Kurkina and Talipova* [2011] reported that the semidiurnal oscillations were observed at high Arctic latitudes over underwater slopes, while only packets of short-period waves were observed far from the slopes over relatively flat bottom. They presented a model confirming this.

Observations reported by *Morozov and Paka* [2010] show that only packets of short-period internal waves were observed over almost flat slopes in the Kara Sea. Influence of the critical latitude on tidal internal waves of frequency M_2 (period 12.4 hours) is shown on the example of moored measurements. North of 74.5° N, the temperature spectra reveal only the S_2 peak (period 12.0 h), while the current spectra show two peaks M_2 and S_2 [*Morozov*, 2023]. Many observations of short-period internal waves in the study region in the Fram Strait north of the critical latitude were also observed from satellite observations [*Kozlov et al.*, 2024]. The observations of short-period internal waves in the Fram Strait may indicate the existence and further decay of internal tide, as suggested in the work of *Vlasenko et al.* [2003], confirming the main conclusion of this paper.

It was shown by *Vlasenko et al.* [2003] that at high latitudes nonlinearity should be high to allow generation of internal waves otherwise, nonlinear effects are suppressed by rotation. The authors demonstrate that such generation is possible if the problem has a nonlinear formulation. They suggested a numerical nonlinear model, which allows generation of internal tide at high latitudes and its breaking into packets of short-period internal wave during a specific phase of internal tide, when conditions for its breaking are formed.

The problem of existence of internal tides near the critical latitude has been analyzed by *Morozov* [2023] and *Morozov et al.* [2008] based on a numerical model developed by *Vlasenko* [1992]. As a result of calculations and analysis, a map of the amplitudes of semidiurnal internal tidal waves in the Arctic seas has been constructed. The maximum amplitudes of internal tidal waves occur over underwater slopes.

Very large amplitudes of internal tides were found in the Kara Gates. Internal waves in the Kara Gates Strait were studied using moored measurements and towed CTD-profilers in the scanning mode. Internal waves turned out to be extremely large and their dynamics is close to the similar waves in the Strait of Gibraltar. Waves with heights of up to 40 m were directed towards the Barents Sea. Similarly to the Fram Strait, internal tidal waves in the Kara Gates Strait are also accompanied by the formation of short, large-amplitude internal waves [*Kozlov et al.*, 2023]. The opposing current east of the strait decreases the wavelength, and, consequently, the amplitude of internal waves increases.

Data and Methods

We analyzed long term moorings in the Fram Strait at 79° N. Oceanography of the region has been intensely studied using deployments of moorings and CTD sections [*Beszczynska-Möller et al.*, 2012; *Fahrbach et al.*, 2001]. In this paper, we analyze temperature measurements at moorings at three points in the Fram Strait in 1997–1999 carried out under the ASOF international project (https://asof.awi.de/science/projects/13-monitoring-of-oceanic-fluxes-across-fram-strait/) by scientists from the Norwegian Polar Institute and German Alfred Wegener Institute. A line of moorings was deployed approximately along 79° N across the Fram Strait from Spitsbergen to Greenland (Figure 2).

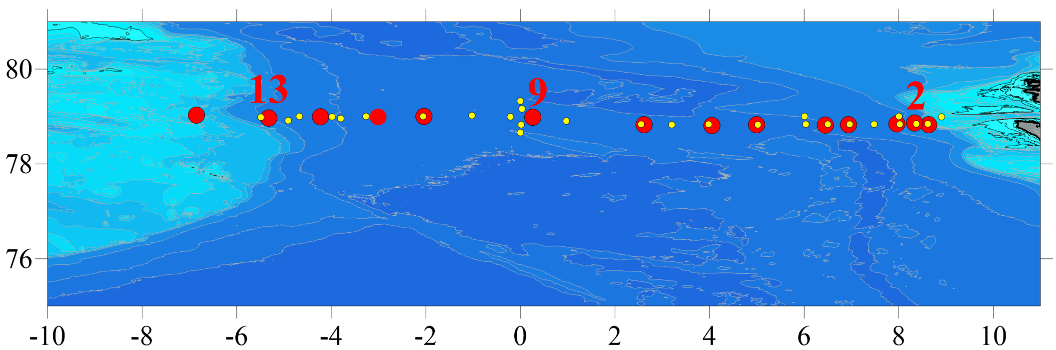

Figure 2. Chart of moorings (red dots with numbers) and CTD stations (yellow dots) in the Fram Strait.

The eastern and western moorings were located on the slope while central moorings were on a relatively flat bottom of the strait. The moorings were equipped with 3 to 6 Aanderaa RCM current and temperature meters at depths from 200 m to the bottom. Time sampling was either 1 or 2 hours. Data in the Fram Strait are freely available on the website [*Fahrbach et al.*, 2012a,b,c]. We also used satellite altimetry for estimating vorticity in the region. The most attention in the analysis was focused on three moorings deployed on the slopes of the strait and in the middle (Figure 3).

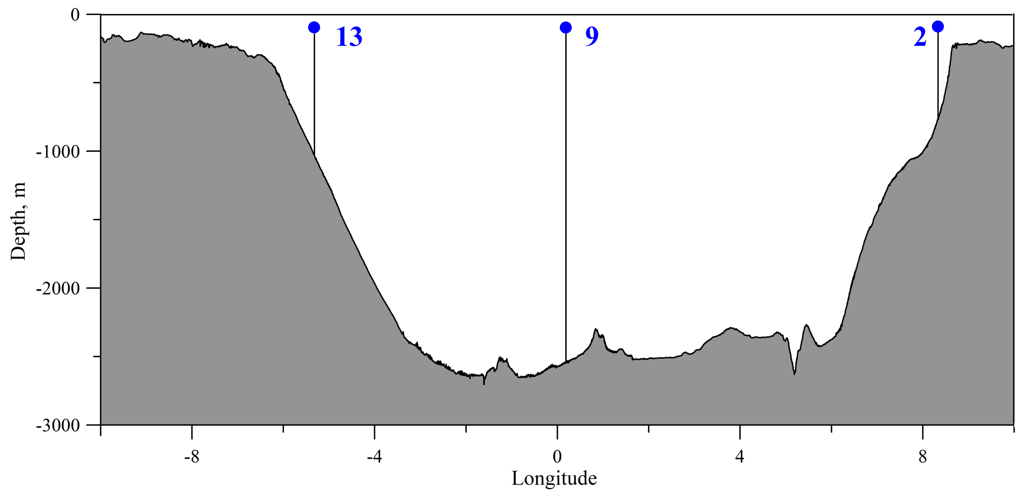

Figure 3. Depth profile across the Fram Strait along 79° N, and scheme of moorings 13, 9, and 2 (from left to right).

Results

The region is characterized by several currents. Warm West Spitsbergen Current is a continuation of the North-Atlantic Current. Its western branch crosses the Norwegian Sea and flows to the Arctic along the west Spitsbergen coast. In the middle of the Fram Strait part of the current makes a retroflection loop and turns west and then south. The cold East Greenland Current flows along the eastern coast of Greenland to the south. Current vectors at the surface based on satellite altimetry are shown in Figure 4.

Roughly in the central part of the strait, vorticity is often anticyclonic, as a topographically trapped large anticyclone often forms here. The mooring line along 79° N passes through its southern periphery, and a cyclonic eddy usually forms slightly south of it. This is shown in [*Kozlov et al.*, 2020].

One can see from Figure 4 that anticyclonic vorticity exists in the western part of the section along 79° N. Both cyclonic and anticyclonic (in the north) and cyclonic (in the south) rotations are seen in the central part of the strait, and cyclonic vorticity exists in the east and south of 79° N. Cyclonic meander of the West Spitsbergen Current determines cyclonic vorticity south of the line of moorings, but sometimes the meander fluctuates to the north; thus, bringing cyclonic rotation to the mooring line.

We analyzed vorticity based on satellite altimetry in three regions of the Fram Strait: western, central, and eastern. Unfortunately, the western region is often covered with ice; thus, vorticity remains undetermined. Long-term variations in vorticity in the eastern and central parts of the section are shown in Figure 5. One can easily see from Figures 4, 5 that vorticity in the central part of the strait is less intense than in the eastern and western parts of the section. A thin line in Figure 5 shows a negative vorticity of 0.00002 s^{-1}, which is needed to make denominator in Equation 1 positive at latitude 79° N. The greater absolute values of negative vorticity are colored blue in the figure.

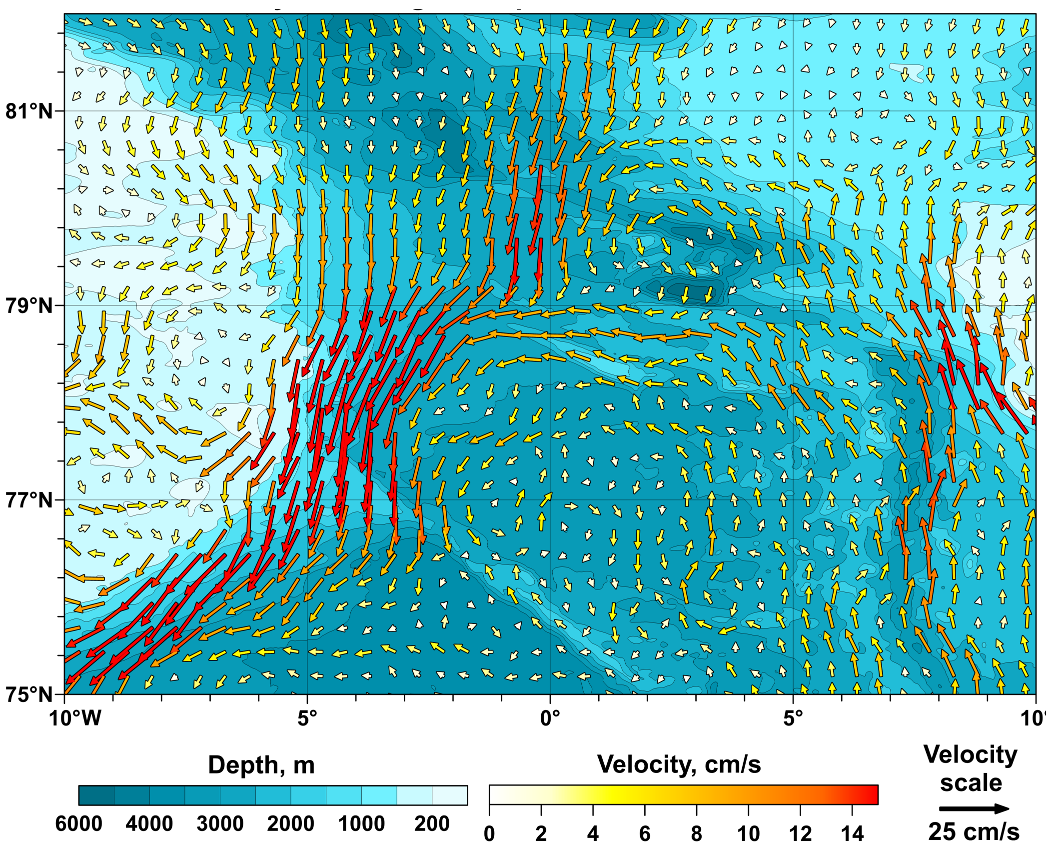

Figure 4. Geostrophic currents at the surface based on the mean satellite altimetry over 1993–2012 of the sea surface height above geoid [*European …*, 2020].

Forcing from the barotropic tide that generates internal tides was different over the section. Figures of tidal ellipses based on the TPXO9 model is shown in Figure 6. The dates were selected especially for the spring tides.

Central region. Let us analyze temperature measurements on mooring 9 in the middle of the section. The mooring was deployed at 78.99° N, 0.27° W. One can see from Figure 5 that vorticity in March 1999 reached $-0.000122\,\mathrm{s}^{-1}$. The local Coriolis frequency at 79° N is $0.000022\,\mathrm{s}^{-1}$. If local negative vorticity is added to the Coriolis frequency, the efficient Coriolis frequency becomes smaller than the M_2 frequency and appearance of the M_2 internal tide is possible with such high negative vorticity. In February and April of 1999, vorticities in this region were cyclonic (positive). A spectrum of temperature fluctuations shows a reliable peak at the M_2 frequency (0.0806 cph) in March and no peaks in February and April (Figure 7).

Eastern region. Next, we analyze temperature measurements on mooring 2 in the eastern part of the section. The mooring was deployed at 78.86° N, 8.33° E. One can see from Figure 5 that vorticity in May 1998 reached $-0.000521\,\mathrm{s}^{-1}$ giving a possibility for the M_2 internal tide to appear. In February and August 1998, vorticities in this region were cyclonic (positive). A spectrum of temperature fluctuations shows a reliable peak at the M_2 frequency (0.0806 cph) in March and no peaks in February and August (Figure 8).

Western region. We continue analyzing temperature measurements on mooring 13 in the western part of the section. The mooring was deployed at 78.95° N, 5.35° W.

During two months, vorticity in the western region was negative. However, in the end of April, the maximum absolute value increased. Even though vorticity in January

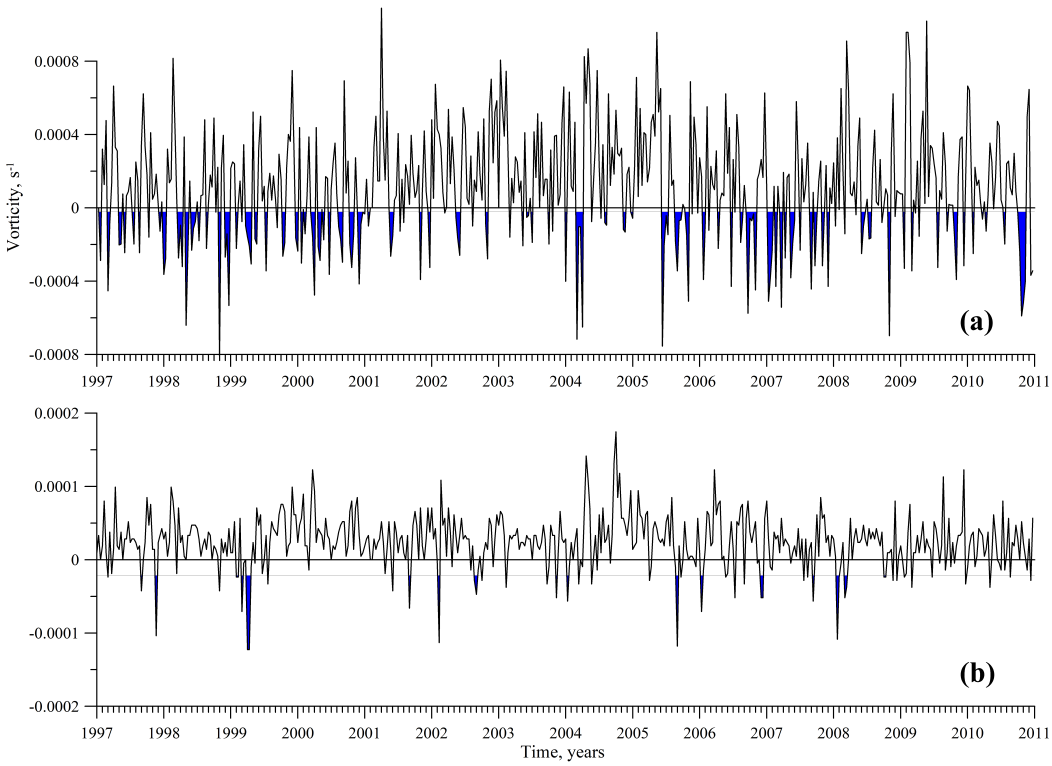

Figure 5. Vorticity versus time in the eastern part of the section (top panel, a) and central part of the section (bottom panel, b). Graph below vorticity $-0.00002\,\mathrm{s}^{-1}$ is shown in blue color.

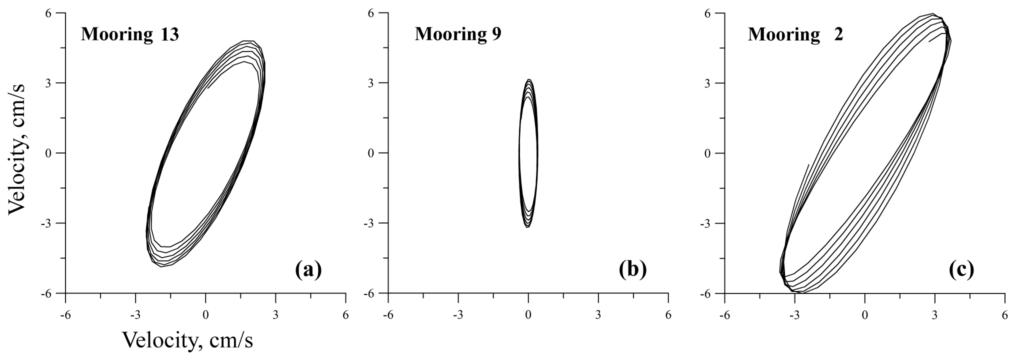

Figure 6. Tidal ellipses of the M_2 and S_2 tides in three regions of the Fram Strait. The dates of the estimates correspond to spring tides on March 31–April 2, 1999. Velocities are in cm/s. Coordinates of moorings: western mooring F13, 78.95° N, 5.35° W (a); central mooring F9, 78.99° N, 0.27° W (b); and eastern mooring F2, 78.86° N, 8.33° E (c).

and August 1999 was negative, the peak of temperature fluctuations appeared only in the time series related to the second half of April (Figure 9). Spectra of temperature fluctuations shows a reliable peak at the M_2 frequency (0.0806 cph) only in April 1999 and no peaks in January and August 1999 (Figure 10). We note that mooring 13 was located on the continental slope, where forced internal tides are possible. However, peaks on the spectrum appeared only when vorticity became strongly negative.

Discussion

We estimated vorticity of waters induced by mean currents assuming that the horizontal scale of vorticity is 20,000 m. Vorticity was estimated from the satellite altimetry data and is related to the surface layer. We analyzed moored temperature spectra at depths of 200–250 m The moorings were deployed in a line across the strait. We specified the

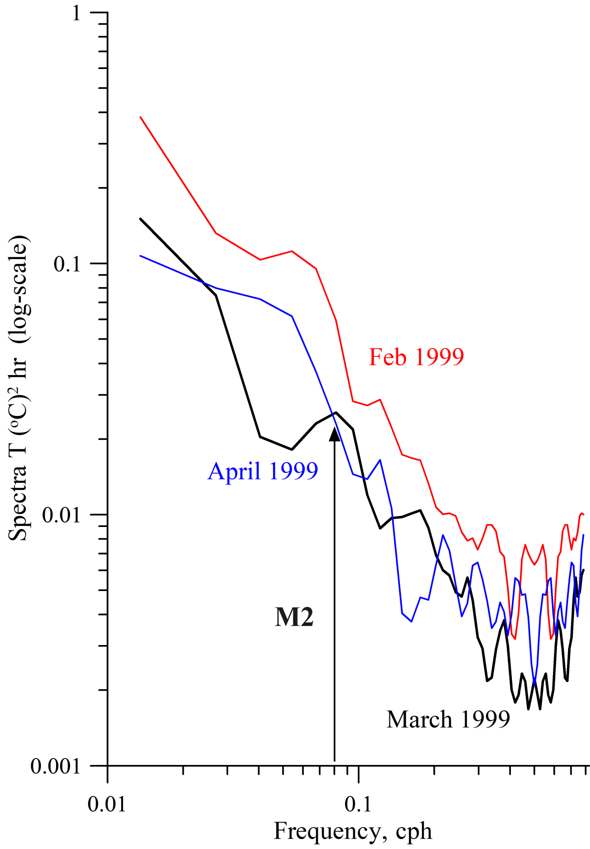

Figure 7. Frequency spectra of temperature fluctuations at mooring 9 (78.99° N, 0.27° W) in February (red), March (black), and April (blue) 1999. The spectrum in March is characterized by a peak at the M_2 frequency (0.0806 cph).

scale two times larger (40,000 km), but the variations in vorticity principally did not differ strongly from those calculated at a horizontal scale of 20,000 m. If we decrease the scale twice, too much noise appears in the vorticity data. This is because a scale of 20–40 km is close to the Rossby radius for this region. Smaller distances for estimating vorticity results in greater noise.

We judge the existence of internal tides based on the temperature measurements on moorings in the Fram Strait. Intensity of internal tides was estimated based on the fluctuations of velocity and temperature at the M_2 frequency on three moorings.

We continue our research by analyzing the amplitudes and energy of internal tide in the western, central, and eastern parts of the section in August 1998. The energy densities of internal tide (ETW) were averaged over the wave period according to [*Holloway and Merrifield*, 1999; *Lozovatsky et al.*, 2003; *Torgrimson and Hickey*, 1979]. We used a band-pass filter to separate semidiurnal tidal components from the velocity and temperature time series. The density of the kinetic energy of the horizontal components of internal tide was determined as a sum of squared amplitudes of velocity. The total energy density of internal tide was calculated using the following formula:

$$E_{TW}(z) = 0.25\,\rho\left(\overline{u_{IT}^2(z)} + \overline{v_{IT}^2(z)} + N^2(z)\,\overline{\zeta_{IT}^2(z)}\right)$$

Here, u_{IT}, v_{IT} are the amplitudes of the semidiurnal internal tide velocity components, ζ_{IT} are vertical displacements [*Holloway and Merrifield*, 1999; *Lozovatsky et al.*, 2003; *Torgrimson and Hickey*, 1979]. Internal tide velocity components were calculated from the mooring data. Vertical displacements were calculated from moored velocity measurements divided by the vertical temperature gradient. The vertical temperature gradient and

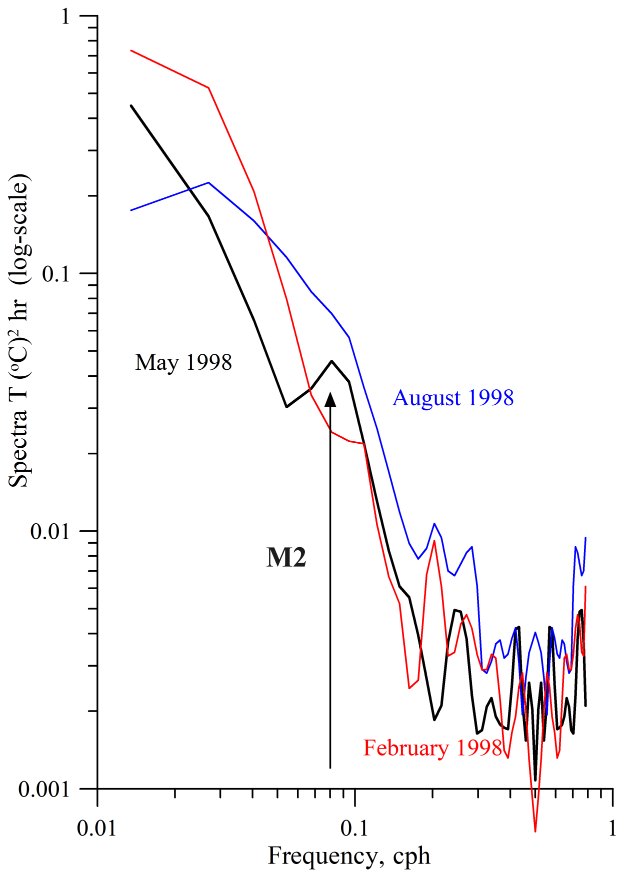

Figure 8. Frequency spectra of temperature fluctuations at mooring 9 (78.99° N, 0.27° W) in February (red), March (black), and April (blue) 1999. The spectrum in March is characterized by a peak at the M_2 frequency (0.0806 cph).

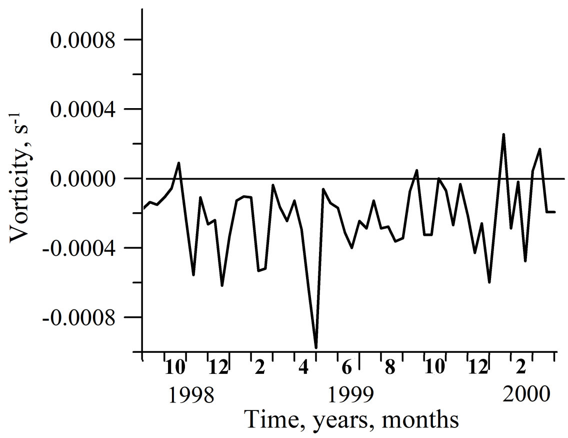

Figure 9. Vorticity versus time in the western region of the section.

vertical distribution of the Brunt–Väisälä frequency were estimated from the CTD casts during one-time survey in the study site. The data were taken from the WOD18 database.

Horizontal velocities of the barotropic tide in the region were calculated using the TPXO9 tidal model based on satellite data assimilation [*Egbert and Erofeeva*, 2002]. The tidal ellipses were oriented in the meridional direction, which is caused by the propagation of tidal currents in the strait. The barotropic tide velocities normal to the slope (east-west components) were within ±3 cm/s in the eastern part and western parts and ±1 cm/s in the

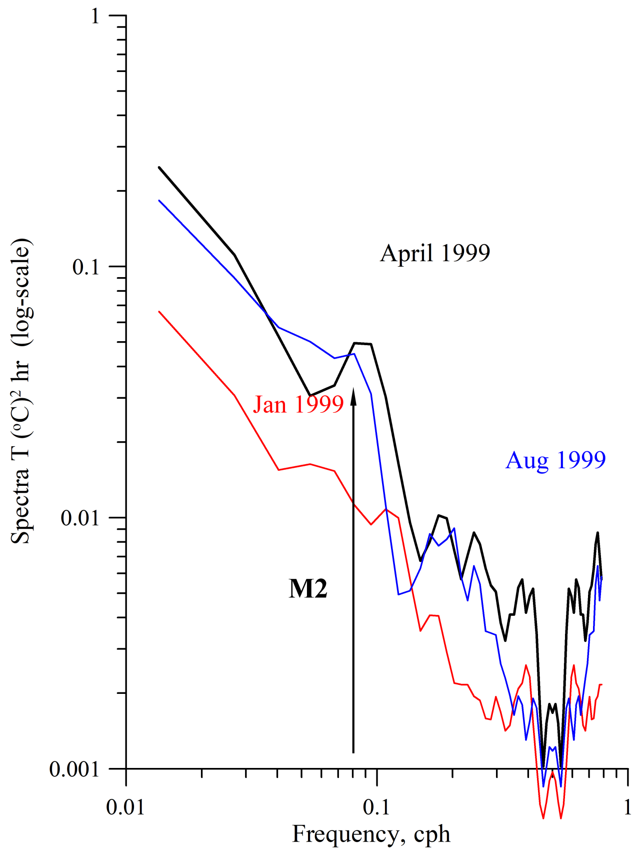

Figure 10. Frequency spectra of temperature fluctuations at mooring 13 (78.95° N, 5.35° W) in January (red), April (black), and August (blue) 1999. The spectrum in April is characterized by a peak at the M_2 frequency (0.0806 cph).

central part. This gives us an idea that forcing of internal tides over slopes in the west and east is stronger than in the central part.

The energy density of internal tides was calculated from the time series one month long in August 1998; thus, we excluded the spring-neap variability. The calculations show that the mean amplitudes of internal tides at a depth of 220–250 m on moorings 13 (west), 9 (center), and 2 (east) decreased from 34 m in the east to 17 m in the center, and 15 m in the west of the strait. The energy on the moorings decreases from east to west as 6.7, 2.4, and 2.0 J/m^3, respectively. Thus, our estimates reveal that internal tides are generated more intensely on the eastern slope of the strait. Generation in the central part and over the western slope is less intense. This may be caused by the fact that tidal currents are directed along the strait. The transversal slope inclinations are more or less the same in the eastern and western parts. The inclinations of the slope across the sections line (which coincides with the transversal sill across the strait) are steeper in the eastern part and flatter in the western one. Thus, tidal currents overflowing the sill generate stronger internal tides in the eastern part. Strong internal waves and missing in the region was reported in [*Fer et al.*, 2020].

The idea that internal tides are stronger in the eastern part of the section is supported by slightly stronger amplitudes of the barotropic tide in the eastern part. Tidal ellipses for the sum of the M_2 and S_2 tides were calculated using the TPXO9 approach based on the satellite altimetry. Tidal ellipses in the eastern part show that tides are stronger there.

This result is supported by not very reliable estimates of comparing the estimated spectra with the Garrett–Munk model (GM-72) [*Garrett and Munk*, 1972]. They are not very reliable because we could estimate the values of the vertical temperature gradient and Brunt–Väisälä frequency based on the CTD profiles taken only once across the strait

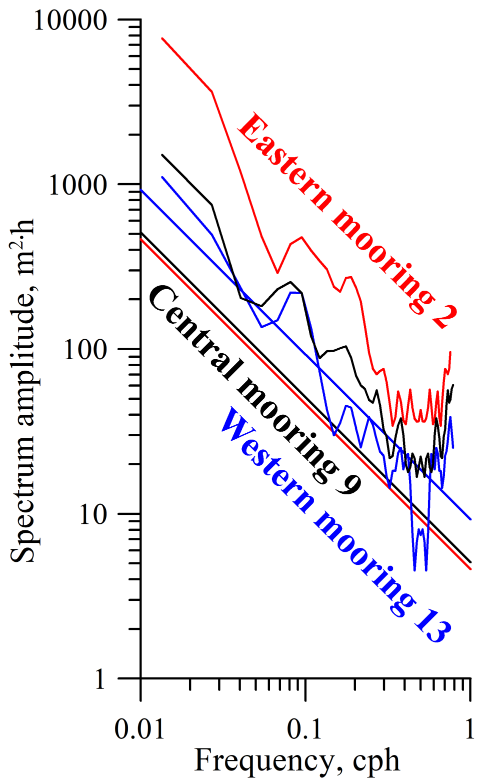

Figure 11. Spectra of vertical displacements from three moorings at depths of 220–250 m. Mooring 13, blue line, mooring 9, black line, mooring 2, red line. The corresponding GM spectra are shown in the same colors.

(Figure 2). Temperature fluctuations on the spectra were recalculated to vertical displacements of water particles by dividing the fluctuations by the vertical temperature gradient from CTD casts. The vertical temperature gradients and Brunt–Väisälä frequences are slightly different in different regions of the section. In addition, the GM model cannot be applied correctly to the Arctic data and to the data from relatively upper layer (220–250 m). However, this comparison confirmed the idea that internal tides are stronger in the eastern part.

Estimates of the Garrett–Munk spectra were performed as follows. The frequency spectra formula from the GM-72 model is written as (MS is the spectrum of vertical fluctuations of water particles):

$$MS(\omega, z) = C_M f \frac{\sqrt{\omega^2 - f^2}}{N(z)\,\omega^3}.$$

Here, C_M is coefficient 204 m^2/h, f is the inertial frequency, ω is the wave frequency, $N(z)$ is the Brunt–Väisälä frequency.

For high-frequency waves, the expression is simplified:

$$MS(\omega, z) = C_M \frac{f}{N(z)} \omega^{-2},$$

and the spectrum of fluctuations of vertical displacements is approximated by an inversely proportional dependence on the square of the frequency.

Figure 11 shows three spectra of vertical displacements: red for the eastern mooring, black for the central mooring, and blue for the western mooring. The GM spectra for each region are shown in the same colors. The lines of the GM spectra are different because the estimates of the Brunt–Väisälä frequency are different in different parts of the strait.

Conclusions

We revealed that spectral peaks on the moored temperature spectra in different regions of the Fram Strait appear when anticyclonic vorticity is present in the velocity field of surface currents. Intensity of internal waves based only on the temperature spectra does not change strongly regardless the existence or absence of the tidal peak on the spectra. Generation of internal tide is stronger over the Spitsbergen slope than in the center of the strait and over the Greenland slope. Finding of regions with intense internal tides is helpful for estimation the regions with high mixing.

Acknowledgements. This research was supported by Russian Science Foundation, grants 23-77-30001 (analysis of long term measurements) 25-17-00309 (interpretation of results).

References

Baines P. G. On internal tide generation models // Deep Sea Research Part A. Oceanographic Research Papers. — 1982. — Vol. 29, no. 3. — P. 307–338. — https://doi.org/10.1016/0198-0149(82)90098-x.

Beszczynska-Möller A., Fahrbach E., Schauer U., et al. Variability in Atlantic water temperature and transport at the entrance to the Arctic Ocean, 1997-2010 // ICES Journal of Marine Science. — 2012. — Vol. 69, no. 5. — P. 852–863. — https://doi.org/10.1093/icesjms/fss056.

Egbert G. D. and Erofeeva S. Efficient Inverse Modeling of Barotropic Ocean Tides // Journal of Atmospheric and Oceanic Technology. — 2002. — Vol. 19, no. 2. — P. 183–204. — https://doi.org/10.1175/1520-0426(2002)019<0183:eimobo>2.0.co;2.

European Union-Copernicus Marine Service, Global Ocean Mean Dynamic Topography. — Mercator Ocean International, 2020. — https://doi.org/10.48670/MOI-00150. — (Accessed on 23-02-2025).

Fahrbach E., Meincke J., Østerhus S., et al. Direct measurements of volume transports through Fram Strait // Polar Research. — 2001. — Vol. 20, no. 2. — P. 217–224. — https://doi.org/10.1111/j.1751-8369.2001.tb00059.x.

Fahrbach E., Rohardt G. and Schauer U. Physical oceanography and current meter data from mooring F13-3. — 2012a. — https://doi.org/10.1594/PANGAEA.800306.

Fahrbach E., Rohardt G. and Schauer U. Physical oceanography and current meter data from mooring F2-2. — 2012b. — https://doi.org/10.1594/PANGAEA.800330.

Fahrbach E., Rohardt G. and Schauer U. Physical oceanography and current meter data from mooring F9-1. — 2012c. — https://doi.org/10.1594/PANGAEA.800408.

Fer I., Koenig Z., Kozlov I. E., et al. Tidally Forced Lee Waves Drive Turbulent Mixing Along the Arctic Ocean Margins // Geophysical Research Letters. — 2020. — Vol. 47, no. 16. — https://doi.org/10.1029/2020GL088083.

Garrett C. and Kunze E. Internal tide generation in the deep ocean // Annual Review of Fluid Mechanics. — 2007. — Vol. 39, no. 1. — P. 57–87. — https://doi.org/10.1146/annurev.fluid.39.050905.110227.

Garrett C. and Munk W. Space-Time scales of internal waves // Geophysical Fluid Dynamics. — 1972. — Vol. 3, no. 3. — P. 225–264. — https://doi.org/10.1080/03091927208236082.

Holloway P. E. and Merrifield M. Internal tide generation by seamounts, ridges, and islands // Journal of Geophysical Research: Oceans. — 1999. — Vol. 104, no. C11. — P. 25937–25951. — https://doi.org/10.1029/1999jc900207.

Khimchenko E. E., Frey D. I. and Morozov E. G. Tidal internal waves in the Bransfield Strait, Antarctica // Russian Journal of Earth Sciences. — 2020. — Vol. 20, no. 2. — ES2006. — https://doi.org/10.2205/2020es000711.

Konyaev K. V., Plueddemann A. and Sabinin K. D. Internal tide on the Yermak Plateau in the Arctic Ocean // Izvestiya, Atmospheric and Oceanic Physics. — 2000. — Vol. 36, no. 4. — P. 500–509.

Konyaev K. V. and Sabinin K. D. Waves in the Ocean. — Leningrad : Gidrometeoizdat, 1992. — 272 p. — (In Russian).

Kozlov I. E., Kopyshov I. O., Frey D. I., et al. Multi-Sensor Observations Reveal Large-Amplitude Nonlinear Internal Waves in the Kara Gates, Arctic Ocean // Remote Sensing. — 2023. — Vol. 15, no. 24. — https://doi.org/10.3390/rs15245769.

Kozlov I. E., Mihailichenko T. V. and Petrenko L. A. Properties of Short-Period Internal Waves Near Svalbard from Sentinel-1 Satellite Data // Russian Journal of Earth Sciences. — 2024. — Vol. 24. — ES5008. — https://doi.org/10.2205/2024es000951.

Kozlov I. E., Plotnikov E. V. and Manucharyan G. E. Brief Communication: Mesoscale and submesoscale dynamics in the marginal ice zone from sequential synthetic aperture radar observations // The Cryosphere. — 2020. — Vol. 14, no. 9. — P. 2941–2947. — https://doi.org/10.5194/tc-14-2941-2020.

Kozubskaya G. I., Konyaev K. V., Plueddemann A., et al. Internal waves at the slope of Bear Island from the data of the Barents Sea Polar Front Experiment (BSPF-92) // Oceanology. — 1999. — Vol. 39, no. 2. — P. 147–154.

Krauß W. Interne Wellen (Methoden und Ergebnisse der Theoretischen Ozeanographie: Band II). — Berlin-Nikolasee : Gebrüder Borntraeger, 1966. — 248 p.

Kurkina O. E. and Talipova T. G. Huge internal waves in the vicinity of the Spitsbergen Island (Barents Sea) // Natural Hazards and Earth System Sciences. — 2011. — Vol. 11, no. 3. — P. 981–986. — https://doi.org/10.5194/nhess-11-981-2011.

LeBlond P. H. and Mysak L. A. Waves in the Ocean. — Amsterdam : Elsevier, 1978. — P. 602.

Levine M. D., Paulson C. A. and Morison J. H. Internal Waves in the Arctic Ocean: Comparison with Lower-Latitude Observations // Journal of Physical Oceanography. — 1985. — Vol. 15, no. 6. — P. 800–809. — https://doi.org/10.1175/1520-0485(1985)015<0800:iwitao>2.0.co;2.

Lozovatsky I. D., Morozov E. G. and Fernando H. J. S. Spatial decay of energy density of tidal internal waves // Journal of Geophysical Research: Oceans. — 2003. — Vol. 108, no. C6. — P. 3201–3216. — https://doi.org/10.1029/2001jc001169.

Marchenko A. V. and Morozov E. G. Surface manifestations of the waves in the ocean covered with ice // Russian Journal of Earth Sciences. — 2016. — Vol. 16, no. 1. — ES1001. — https://doi.org/10.2205/2016es000561.

Morozov E. G. Semidiurnal internal wave global field // Deep Sea Research Part I: Oceanographic Research Papers. — 1995. — Vol. 42, no. 1. — P. 135–148. — https://doi.org/10.1016/0967-0637(95)92886-c.

Morozov E. G. Wave Processes in the Arctic // Processes in GeoMedia-Volume VI. Vol. 6. — Springer International Publishing, 2023. — P. 175–203. — https://doi.org/10.1007/978-3-031-16575-7_18.

Morozov E. G., Ansorge I. and Vinokurov D. V. Semidiurnal internal tide in the Atlantic Ocean // Russian Journal of Earth Sciences. — 2020. — Vol. 20, no. 4. — ES4005. — https://doi.org/10.2205/2020es000733.

Morozov E. G. and Frey D. I. Strait of Kara Gates: A Region of Strong Internal Tides in the Arctic Seas // Russian Journal of Earth Sciences. — 2023. — Vol. 23. — ES3005. — https://doi.org/10.2205/2023es000860.

Morozov E. G. and Paka V. T. Internal waves in a high-latitude region // Oceanology. — 2010. — Vol. 50, no. 5. — P. 668–674. — https://doi.org/10.1134/S0001437010050048.

Morozov E. G., Paka V. T. and Bakhanov V. V. Strong internal tides in the Kara Gates Strait // Geophysical Research Letters. — 2008. — Vol. 35, no. 16. — https://doi.org/10.1029/2008gl033804.

Morozov E. G. and Pisarev S. V. Internal tides at the Arctic latitudes (numerical experiments) // Oceanology. — 2002. — Vol. 42, no. 2. — P. 153–161.

Morozov E. G. and Pisarev S. V. Internal Waves in the Region of the Akselsundet Strait of Western Spitsbergen Island // Izvestiya, Atmospheric and Oceanic Physics. — 2023. — Vol. 59, no. 4. — P. 432–442. — https://doi.org/10.1134/s0001433823040126.

Parsons A. R., Bourke R. H., Muench R. D., et al. The Barents Sea Polar Front in summer // Journal of Geophysical Research: Oceans. — 1996. — Vol. 101, no. C6. — P. 14201–14221.

Pisarev S. V. Experimental frequency spectra of internal waves in an ice-covered high-latitude basin // Oceanology. — 1988. — Vol. 28, no. 5. — P. 577–580.

Pisarev S. V. Some measurements of the spatial and temporal characteristics of internal waves in an ice-covered high-latitude basin // Oceanology. — 1991. — Vol. 31, no. 1. — P. 42–46.

Pisarev S. V. Spatial and temporal characteristics of internal waves at the edge of the continental shelf in the Arctic basin // Oceanology. — 1992. — Vol. 32, no. 5. — P. 579–583.

Plueddemannn A. J., Krishfield R., Takizawa T., et al. Upper-ocean velocities in the Beaufort Gyre // Geophysical Research Letters. — 1998. — Vol. 25, no. 2. — P. 183–186. — https://doi.org/10.1029/97gl53638.

Prinsenberg S. J., Wilmot W. L. and Rattray M. Generation and dissipation of coastal internal tides // Deep Sea Research and Oceanographic Abstracts. — 1974. — Vol. 21, no. 4. — P. 263–281. — https://doi.org/10.1016/0011-7471(74)90098-9.

Tareev B. A. On the dynamics of internal gravity waves in a constantly stratified ocean // Izv. Akad. Nauk, Fiz. Atmos. Okeana. — 1966. — Vol. 2, no. 10. — P. 1064–1075. — (In Russian).

Torgrimson G. M. and Hickey B. M. Barotropic and Baroclinic Tides over the Continental Slope and Shelf off Oregon // Journal of Physical Oceanography. — 1979. — Vol. 9, no. 5. — P. 945–961. — https://doi.org/10.1175/1520-0485(1979)009<0945:babtot>2.0.co;2.

Vlasenko V., Stashchuk N., Hutter K., et al. Nonlinear internal waves forced by tides near the critical latitude // Deep Sea Research Part I: Oceanographic Research Papers. — 2003. — Vol. 50, no. 3. — P. 317–338. — https://doi.org/10.1016/s0967-0637(03)00018-9.

Vlasenko V. I. Non-linear model for the generation of baroclinic tides over extensive inhomogeneities of the seabed relief // Soviet Journal of Physical Oceanography. — 1992. — Vol. 3, no. 6. — P. 417–424. — https://doi.org/10.1007/bf02197556.